Hyaluronic acid-based hydrogels as codelivery systems: the effect of intermolecular interactions investigated by HR-MAS and solid-state NMR Spectroscopy

Valeria Vanoli[a], Mosè Casalegno[a,*], Marina Carravetta[b], Fabio Pizzetti[a], Andrea Mele[a], Filippo Rossi[a], Franca Castiglione[a,*]

[a] *Dipartimento di Chimica, Materiali e Ingegneria Chimica "G. Natta", Politecnico di Milano, via Mancinelli 7, I-20131 Milano (MI), Italy*

[b] *School of Chemistry, University of Southampton, Southampton, SO17 1BJ (UK)*

* Corresponding authors

Email: mose.casalegno@polimi.it , franca.castiglione@polimi.it

Abstract

Hydrogels based on hyaluronic acid and agarose-carbomer, due to their peculiar 3D architecture and biocompatibility, are promising candidates for pharmaceutical strategies based on the codelivery of drugs targeting different diseases. The successful development of these applications requires a precise understanding of drug-drug interactions and their effects on transport and release mechanisms. In this study, such an investigation is carried out on hydrogels loaded with ethosuximide and sodium salicylate at different concentrations. Intermolecular interactions and transport properties are characterized by means of High Resolution Magic Angle Spinning and solid-state Magic Angle Spinning NMR Spectroscopy.

At variance with our previous findings on single-drug formulations, the two drugs exhibit closely similar diffusion patterns when co-loaded in the HA-based hydrogels, plausibly due to drug-drug intermolecular interactions. At the highest drug concentrations, where superdiffusion comes into play, we find a fraction of molecules with time-varying diffusion coefficients. A trapping-release mechanism is proposed to explain this observation, which also accounts for the role of drug-hydrogel interactions in drug diffusion motion. The effects of drug-drug interactions on release profiles is finally assessed by means of *in vitro* release experiments.

Keywords: Hydrogels; HR-MAS NMR Spectroscopy; drug codelivery; diffusion.

1. Introduction

Controlled drug delivery systems (DDS) are designed to release active pharmaceutical ingredients gradually over time, at a rate chosen to maximize the therapeutic response (Hoffman, 2008; Bajpai et al., 2008). In contrast to conventional drug administration routes, which require high dosages due to uneven drug release and distribution, DDS aim at optimizing drug bioavailability. The benefits associated with their adoption are several (Adepu, & Ramakrishna, 2021), the most important probably being the reduction of the side effects associated with overdosage.

Hydrogels based on natural polysaccharides, such as cellulose (Zong et al., 2022), chitosan (Hamedi et al., 2018), starch (Sethi et al, 2020), sodium alginate (Ji et al., 2021) and hyaluronic acid (HA) are amongst the most versatile DDS, and have been extensively exploited in many clinical formulations for the controlled delivery of synergic drugs (Zhang et al., 2023), therapeutic biomolecules (Rial-Hermida et al., 2021) and tissue engineering (Sahranavard et al., 2020).

The development of HA-based DDS is especially appealing, HA being one of major components of extracellular matrix and biological fluids (Fraser, Laurent, & Laurent, 1997). Hydrogels made by HA alone find limited application in drug delivery due to poor mechanical strength and fast degradation rate (Perez et al., 2021). Different chemical modifications and crosslinking strategies (Khunmanee, Jeong & Park, 2017; Madau et al., 2022; Lv et al., 2014; Hassan, Dong, Wang, 2013) have been proposed to obtain HA-based hydrogels with improved mechanical properties and mesh sizes ranging from tens of nanometers up to a few microns.

One such strategy, based on HA copolymerization has been used by our group to develop and study DDS obtained by mixing HA with agarose-carbomer polymers (Pizzetti et al., 2021; Vanoli et al., 2023).

So far, HA-containing formulations have been successfully exploited in single drug delivery (Huang & Huang, 2018; Noreen et al., 2022). More recently, the possibility to deliver multiple drugs to different target sites has been suggested as a potential way to improve the effectiveness of cancer therapies (Chen, Miller, Dhal, 2014; Gadde, 2015; Meng, Cong, Hu, & Xu, 2020). The same approach, also known as codelivery, has also been evaluated in the treatment of inflammatory diseases (Burmester, Pope, 2017), and can be, in principle, extended to the simultaneous treatment of different, unrelated diseases. The benefits of this approach are clear: a significant improvement of the condition of all patients taking multiple medications, especially those facing chronic diseases (Adepu, & Ramakrishna, 2021; Vargason, Anselmo, & Mitragotri, 2021).

Although attractive, putting this idea into practice requires a precise understanding of the effects of codelivery on drug delivery, adsorption, distribution, and metabolism (Jia et al., 2009; Hu, Sun, Wang & Gu, 2016, Venoruso et al., 2024). A former issue is represented by the need to understand how the simultaneous presence of multiple drugs may impact the diffusion and the release of two or more species, in comparison with the corresponding single drug formulations. Molecular diffusion through the porous network of the hydrogel mainly occurs within the water-rich regions of the gels. It is a complex phenomenon, affected by many factors, such as solute concentration, degrees of gel swelling and cross-linking density, and drug-polymer interactions (Castiglione et al., 2019; Axpe et al., 2019). Beside those factors, the effects of drug-drug interactions should also be considered when two or more drugs are present in the same environment. Depending on their chemical structures, the drugs may negligibly or significantly interact with each other, or with the polymer matrix. Assessing the magnitude of such interactions is challenging and requires the integration of different experimental techniques and careful data processing.

In this work, we attempt to meet this challenge focusing on dual-drugs codelivery in HA-based carbomer-agarose hydrogels. Following the idea introduced above, that multiple drug loading may improve multiple disease treatment, we consider etosuximide and sodium salycilate as probe drugs. Ethosuximide is the drug of choice in the treatment of absence seizures, a form of epilepsy characterized by brief loss of consciousness. This drug is not bound to serum proteins and is metabolized hepatically (80%) into inactive metabolites, primarily by CYP3A4 enzymes [Patsalos et al., 2008]. The interactions of ethosuximide with other drugs has been the subject of some studies [Giaccone et al., 1996; van Wieringen & Vrijlandt, 1983; Bachmann & Jauregui, 1993]. Phenytoin, carbamazepine, and phenobarbital are known to accelerate ethosuximide excretion [Giaccone et al., 1996]. Isoniazid may reduce ethosuximide metabolism [van Wieringen & Vrijlandt, 1983], whereas rifampicin increases ethosuximide clearance [Bachmann & Jauregui, 1993]. No reports are currently available about the interactions between ethosuximide and sodium salicylate. The latter is well known for its anti-inflammatory activity, although no common agreement has been reached about its mode of action [Amann & Peskar, 2002]. Given the need for additional data about the suitability of this combination, the choice of these drugs is here motivated by the possibility to compare our results with those obtained for analogous single drug formulations (Vanoli et al., 2023).

We employ well-established techniques, namely solid-state and high-resolution magic angle spinning (HR-MAS) NMR spectroscopy (Pivato et al., 2021) to characterize drug-drug and drug-polymer intermolecular interactions and their effects on diffusion and release. Two numerical techniques, recently developed by our group (Di Spirito et al, 203; Vanoli et al., 2023) are used to analyze NMR diffusion data and eventually assess deviations from ordinary diffusion. Such deviations are not expected in samples with low drug concentration and large hydrogel meshes

(Castiglione et al., 2019). However, as we reported recently (Vanoli et al., 2023), they can be observed in as many as other samples, making it necessary to process the data prior reporting the diffusion coefficients. Our analysis is finally complemented by and *in vitro* release experiments, which are meant to provide information on the impact of codelivery of two drugs on their release kinetics.

2. Materials and methods

2.1 Materials

The polymers used are Carbomer 974P (MW = 1 MDa, by Fagron, The Netherlands) and Agarose (MW = 200 kDa, by Invitrogen Corp.). Two different types of hyaluronic acids, purchased from Lifecore Biomedical (USA), sodium hyaluronate 10 K (MW = 10 kDa) and sodium hyaluronate 1 M (MW = 1 MDa) were used. The drugs were sodium salicylate (SAL) and ethosuximide (ESM), purchased from Merk. Deuterium oxide (99.9 % deuterium content) and 3-(trimethylsilyl) propionic-2,2,3,3-d_4 acid sodium salt (TSP) were purchased from Merk. All materials were used as received without further purification.

2.2 Hydrogels synthesis, structure, and drug loading

The primary structure of HA is a linear, negatively charged, glycosaminoglycan composed of D-glucuronic acid and N-acetyl-D-glucosamine units bound by alternating β(1-4) and β(1-3) glycosidic bonds (Jiang, Liang, & Noble, 2011). Due to the large number of carboxyl and hydroxyl groups of the sugar moieties, HA adopts expanded random coil structures under diluted

physiological conditions (Lapčík et al., 1998), but may form three dimensional entangled networks at high concentrations (Scott, Cummings, Brass, & Chen, 1991; Scott, & Heatley, 1999).

As mentioned in the Introduction, HA alone is not suitable for hydrogel preparations, due to the fast degradation rate. Therefore, following our previous works (Pizzetti et al, 2021; Castiglione et al; 2019; Vanoli et al., 2023), we investigated agarose-carbomer-hyaluronic acid hydrogels.

These gels were synthesized starting from three biocompatible polymers: carbomer 974P, agarose and hyaluronic acid (Pizzetti et al., 2021; Vanoli et al., 2023). The procedure consists of the following steps: 1) carbomer 974P (8.3 mg for ACL and 16.6 mg for ACH) was dissolved in PBS solution (5 mL) at 25 ◦C, 2) hyaluronic acid HA (87.6 for ACL and 43.8 for ACH) with two different molecular weights was added and the mixture was stirred for 45 min, until complete dissolution. 3) NaOH 1 N was added to adjust pH to 7.4. 4) Finally, agarose powder (25 mg) was added to both solutions and the resulting systems were subjected to electromagnetic stimulation (500 W irradiated power) heating up to 80 ◦C to induce condensation reactions.

Ethosuximide and sodium salicylate were added simultaneously to the polymeric formulation as aqueous solutions before the cross-linking procedure at a temperature of 50°C. The drugs were loaded at three different concentrations: 5 mg/ml, 40 mg/ml, and 75 mg/ml for NMR samples. For comparison purposes, two additional samples were prepared by loading each drug individually. The samples prepared with 5 mg/ml loadings were further lyophilized for solid state NMR analysis. Table 1 collects all the samples considered in this study, along with the corresponding abbreviations.

The resulting three-dimensional network is nanostructured and exhibits anionic nature due to the high presence of carboxylate groups from esterification reaction between carboxyl groups present in carbomer 974p and hyaluronic acid with hydroxyl groups of agarose and hyaluronic acid. The

mesh size - cross-linking degree of the two investigated gels were 245 nm - $2.7 \cdot 10^{-9}$ mol/cm3 (ACL) and 3024 nm - $0.964 \cdot 10^{-9}$ mol/cm^3 (ACH) (Pizzetti et al., 2021). The chemical structures of the hydrogels and the drugs are displayed in Figure 1.

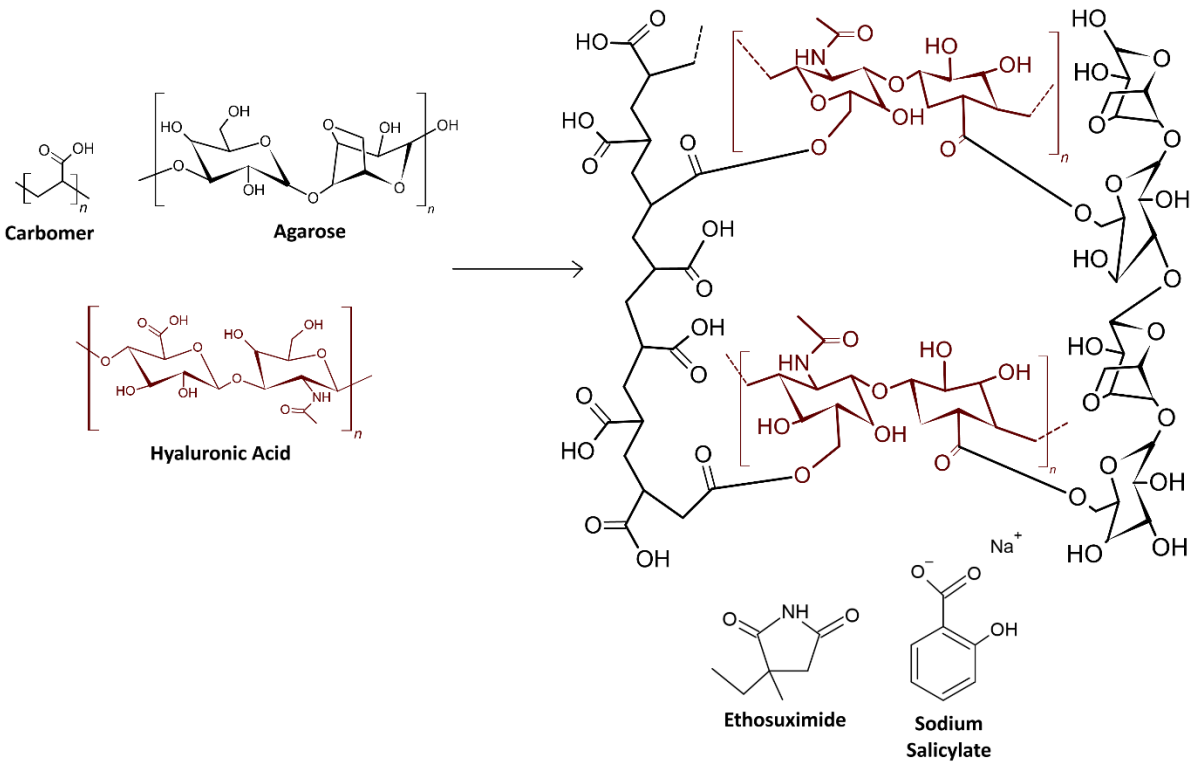

Fig. 1. Chemical structures of the hydrogel's components (carbomer, agarose, hyaluronic acid) and the drugs (ethosuximide and sodium salicylate).

2.3 In vitro release studies

Two samples, ACL-ES05 and ACH-ES05, stored in metal open cylinders (diameter of 0.8 cm and height of 0.7 cm) were submerged in 2 mL of PBS (0.1 M, pH 7.2) at 37 °C, under a 5 % CO_2 atmosphere. 1000 µL of the samples were collected at defined time intervals in the range (5 min-144 h) and the solution was renewed each time adding PBS solution in small amounts. The amount

of drug released was measured using quantitative high resolution NMR Spectroscopy (qNMR). Each measurement was repeated in triplicate.

Table 1. Description of the hyaluronic acid-based hydrogels prepared in this work. The labels E and S are used here to replace ESM and SAL, respectively.

Abbreviation	Drugs amount
ACL-E05	5 mg/mL (ESM)
ACH-E05	5 mg/mL (ESM)
ACL-S05	5 mg/mL (SAL)
ACH-S05	5 mg/mL (SAL)
ACH-ES05	5 mg/mL (ESM) + 5 mg/mL (SAL)
ACL-ES05	5 mg/mL (ESM) + 5 mg/mL (SAL)
ACH-ES40	40 mg/mL (ESM) + 40 mg/mL (SAL)
ACL-ES40	40 mg/mL (ESM) + 40 mg/mL (SAL)
ACL-E40	40 mg/mL (ESM)
ACH-E40	40 mg/mL (ESM)
ACL-S40	40 mg/mL (SAL)
ACH-S40	40 mg/mL (SAL)
ACH-ES75	75 mg/mL (ESM) + 75 mg/mL (SAL)
ACL-ES75	75 mg/mL (ESM) + 75 mg/mL (SAL)

2.4 HR qNMR Spectroscopy

qNMR (Choi et al., 2021) is used to obtain the absolute concentration of a specific compound X from its ^{1}H spectrum. The concentration C_x of the compound X, in the presence of a calibration standard, is calculated according to the equation:

$$C_x = \frac{I_x}{I_{cal}} \cdot \frac{N_{cal}}{N_x} \cdot C_{cal} \quad (1)$$

where I_x, I_{cal}, are the peaks integral of the analyte and the calibrant, respectively, N_x, N_{cal} are the respective number of H nuclei, C_x and C_{cal}, are the concentrations of the analyte x and the calibration standard (cal), respectively. In our analysis, 1.2 mM TSP was used as the internal calibration standard, and the ^{1}H spectra were acquired with 32 K points, SW=10 ppm, 16 scans and 5 s relaxation delay.

2.5 HR-MAS NMR Spectroscopy

The ^{1}H high-resolution magic angle spinning (HR-MAS) NMR spectra of the gel samples were recorded using a Bruker Avance DRX spectrometer operating at 500 MHz proton frequency, equipped with a dual ^{1}H/^{13}C HR-MAS probe head for semisolid samples. Samples were loaded in a 4 mm ZrO_2 rotor containing a volume of about 12 μL. The temperature was set at 305 K with an air flow of 535 L·h^{-1}. All the ^{1}H NMR spectra were acquired with 8 scans, a relaxation delay of 6 s and a spinning rate of 4 kHz.

Self-diffusion coefficients were measured using pulse gradient spin echo (PGSE) methods (Wu, Chen, & Johnson, 1995). A pulsed gradient unit was used to produce magnetic-field pulse gradients up to 53 G·cm^{-1}. The pulse gradients were increased linearly from 2 to 95% of the maximum gradient strength. The duration of the magnetic-field pulse gradients (δ) and the diffusion times (Δ) were optimized for each sample to obtain complete dephasing of the signals with the maximum gradient strength. For the investigated samples, Δ varied from 0.01 s to 0.2 s, while the δ values were in the range of 0.9-3 ms. For each experiment, a series of 40 spectra with 32 K points were collected with 8 scans and a relaxation delay of 12 s.

2.6 Solid state NMR Spectroscopy

Solid-state ^{1}H-^{13}C CP-MAS NMR experiments were carried out for powder samples using a Bruker Avance NEO spectrometer equipped with a commercial 4 mm MAS iProbe. The magnetic field strength was 11.74 T corresponding to a ^{13}C NMR resonance frequency of 125.75 MHz. Samples were packed into 4 mm ZrO_2 rotor and spun at the magic angle with a spinning speed of 12 kHz for all the experiments. ^{13}C CP-MAS spectra were performed with a contact time of 2.5 ms, a repetition time of 5 s and 2000 scans. During acquisition, proton two-phase pulse-modulated decoupling sequence was used. The temperature was set at 298 K.

Fast ^{1}H NMR experiments were performed on an Agilent DD2 600 MHz spectrometer equipped with a 1.6 mm narrow-bore triple resonance T3 probe, at a spinning speed of 36 kHz. Pulse delay was set to 7 s for ACH-ES05 and 4 s for ACL-ES05. Proton NMR spectra were acquired with a background suppression sequence (Patt, 1982). Single Quantum-Double Quantum NMR correlation experiments were recorded using the $R12_2^5$ symmetry-based pulse sequence (Levitt, 2002), a simple 180 pulse R element with phase alternating as ± 75, a nutation frequency of 108 kHz during the recoupling period, and a recoupling time of 333 μs. Two dimensional DQ data were acquired using 40 time increments of 27.7 μs.

2.7 PGSE-NMR theory and data modelling

PGSE-NMR spectroscopy enables the study of molecular diffusion through the application of pulsed magnetic field gradients of varying intensity. Starting at t = 0, the signal intensity of the probed nuclei, I(q,t) decays exponentially over time as follows:

$$I(q,t) = I(0,t) \cdot e^{-\frac{1}{2}q^2\langle z^2(t)\rangle}, \quad (2)$$

where q is the reciprocal space coordinate, defined as $q = (\delta\gamma g)/2\pi$, γ is the magnetogyric ratio of the observed nucleus, g is the field gradient, δ is the gradient pulse, and $\langle z^2(t)\rangle$ represents the mean squared displacement (MSD). The relationship between MSD and time can be generalized as follows:

$$\langle z^2(t)\rangle \sim t^{\alpha} \quad (3)$$

where α is the diffusion exponent. Different values of α can be associated to different diffusion regimes. When $\alpha = 1$, the diffusion is called Fickian, at variance with Fick's laws (Fick, 1855). Deviations of α from one are often classified as subdiffusive ($0 < \alpha < 1$) or superdiffusive ($\alpha > 1$) regimes. In the case, the diffusion is Fickian ($\alpha = 1$) and Gaussian, the previous equation turns into the well-known one (in one dimension):

$$\langle z^2(t)\rangle = 2D \cdot t \quad (4)$$

where D is the diffusion coefficient expressed in m^2/s. Numerical estimates of α and D play an important role in the diffusive behaviour of the probed species. The diffusion time, t, can be related to the NMR data by means of the Stejskal-Tanner equation (Stejskal and Tanner, 1965), for which $t = \Delta - \delta/3$. We note that, owing to the large difference between Δ and δ, we considered $t = \Delta$, in line with our previous studies (Di Spirito et al., 2023).

In this study, two different approaches were adopted to characterize these parameters, namely q-scaling and Gaussian deconvolution (GD). For better clarity, hereafter we briefly resume the main features of both approaches.

The q-scaling approach, recently developed by our group (Casalegno et al. 2017), was used for the calculation of α and the other parameters related to the diffusion mechanism. The q-scaling approach exploits the scaling property of the signal intensity to extract the value of α from a set of

PGSE-NMR measures performed at different diffusion times (t_1, t_2, t_3,….t_N). The scaling property, in this case, can be stated as follows:

$$I\left(q \cdot t_1^{\alpha/2}, t_1\right) = I\left(q \cdot t_2^{\alpha/2}, t_2\right) = I\left(q \cdot t_3^{\alpha/2}, t_3\right) = \ldots = I\left(q \cdot t_N^{\alpha/2}, t_N\right) \quad (5)$$

where, as implied by the equation, the value of α to be determined is that for which all intensities profiles collapse onto a single curve. Given the value of α, the signal intensity can be modelled as:

$$I(q,t) = I(0,t) \cdot e^{-Kt^{\beta} q^{\mu}} \quad (6)$$

where K is a generalized diffusion coefficient with units $\left[m^{\mu} s^{-\beta}\right]$. According to the continuous time random walk theory (Metzler, & Klafter, 2000), the exponents β and μ are associated with the waiting time and the diffusion length of the probed species. Their relationship with α is as follows:

$$\alpha = \frac{2\beta}{\mu} \quad (7)$$

We shall return on the meaning of the latter equation below.

The second numerical technique we propose, the gaussian deconvolution (GD), is used here to calculate the diffusion coefficient, and further quantify the effects of drug-drug and drug-matrix interactions on diffusion. The application of this method, originally based on the Richardson-Lucy algorithm (Lucy, 1974; Richardson, 1972) to NMR diffusion data has been detailed in a recent study. (Di Spirito et al., 2023)

Hereafter, we only resume some fundamental concepts behind this approach, which serve to correctly frame our results. The GD approach assumes that anomalous diffusion may result from a superposition of independent gaussian diffusion processes, characterized by different diffusion coefficients. This assumption is based on the fact the diffusing species may experience different local environments, either due to the interactions between them or with the hydrogel, and turns out

to be realistic in heterogeneous systems, like those here investigated. Mathematically, the distribution of the diffusion coefficients accessed by the diffusant molecules over time can be described by a probability distribution function, P(D). According to this interpretation, the diffusion observed on a macroscopic scale is a statistical average of all individual molecular contributions. Therefore, the signal intensity can be written as:

$$I(q,t) = \int P(D)\, e^{-\frac{1}{2}q^2 D \cdot t} dD \quad (8)$$

Similarly, the diffusion coefficient can be obtained as:

$$D_P = \int P(D) D dD \quad (9)$$

Although the functional form of P(D) is not known, a numerical approximation can be obtained by fitting the experimental signal intensity. In the present work, 300 gaussian functions were used to fit the signal intensities (see Eq.(7)), with diffusion coefficients logarithmically spaced between a minimum (10^{-11} m^2/s) and a maximum (10^{-7} m^2/s) value. Details about the numerical implementation of this approach can be found in Ref. (Di Spirito et al., 2023).

3. Results and discussion

3.1 HR-MAS NMR

Figure 2 reports the ^{1}H HR-MAS spectra of the individual drugs (panel A and panel C) and both drugs (panel B) loaded in ACL gels. The spectra show well resolved lines for all the small molecules enclosed in the polymeric scaffolds. As expected, the spectral contribution of the polymer is filtered off by the HR-MAS acquisition, leaving a clear and well resolved spectrum of the drugs only. This is the ideal situation for a thorough NMR monitoring of the structural and dynamic properties of the drugs in the actual drug-delivery formulation, free from spectral overlap with the signals of the scaffold. Figure 2 displays a clear upfield chemical shift variation (0.05-0.1

ppm) for all the ESM signals on passing from single drug in gel to the formulation containing both drugs at the same concentration (40 mg/mL). A more pronounced shift (0.14-0.2 ppm) is observed at higher drug concentration (75 mg/mL) loaded in gel (Fig. SI1). Conversely, no chemical shift changes are induced on SAL resonances by the presence of ESM in gel. As suggested by our solid-state measurements (see below), the chemical shift variations on ESM protons are likely due to ring current magnetic effects associated to the aromatic-aliphatic interactions between SAL and ESM. Similar results were obtained for ACH formulations.

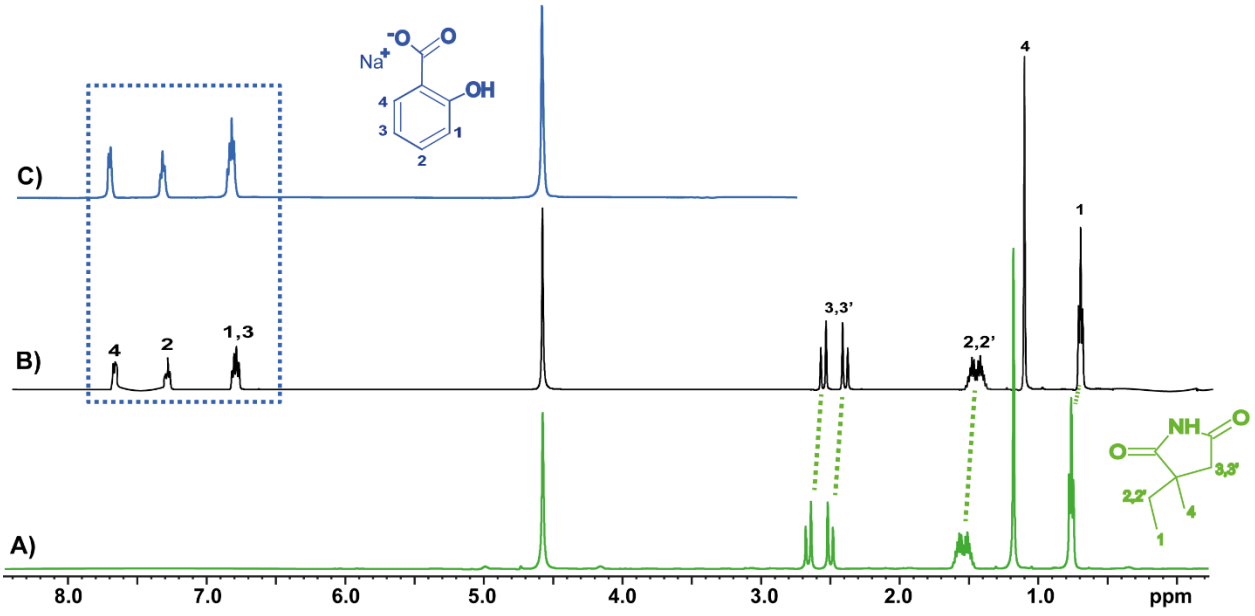

Fig. 2. ^{1}H HR-MAS NMR spectra of A) ACL-E40, B) ACL-ES40 and C) ACL-S40.

3.2 Solid state NMR

To further investigate drug-drug and drug-polymer intermolecular interactions, solid state ^{13}C cross polarization-magic angle spinning (CP-MAS), as well as ^{1}H fast MAS NMR direct acquisition and 2D homonuclear double-quantum NMR techniques were used.

The ^{13}C CP-MAS spectra of HA, carbomer and ACL formulation are shown in Fig. 3 while the ^{13}C CP-MAS spectra of ESM, ACL-E05, SAL, ACL-S05 and ACL-ES05 are shown in Fig. 4. The assignment of ^{13}C chemical shifts of HA/agarose, carbomer and both drugs in the CP-MAS spectra was based on previous works (Rampratap et al. 2023; Vachon & Nairn, 1998) and is also shown in the figures. In Fig. 3a, all ^{13}C signals, corresponding to the chemical shifts of glucose units from HA/agarose and the methyl group (8) at 24 ppm, have been identified. Similarly, in Fig. 3b, the chemical shifts of 183 ppm and 50–25 ppm are assigned to the carboxyl and CH-CH_2 of carbomer. In all spectra, broad lines are observed for hyaluronic acid/agarose and carbomer due to the amorphous character of these materials.

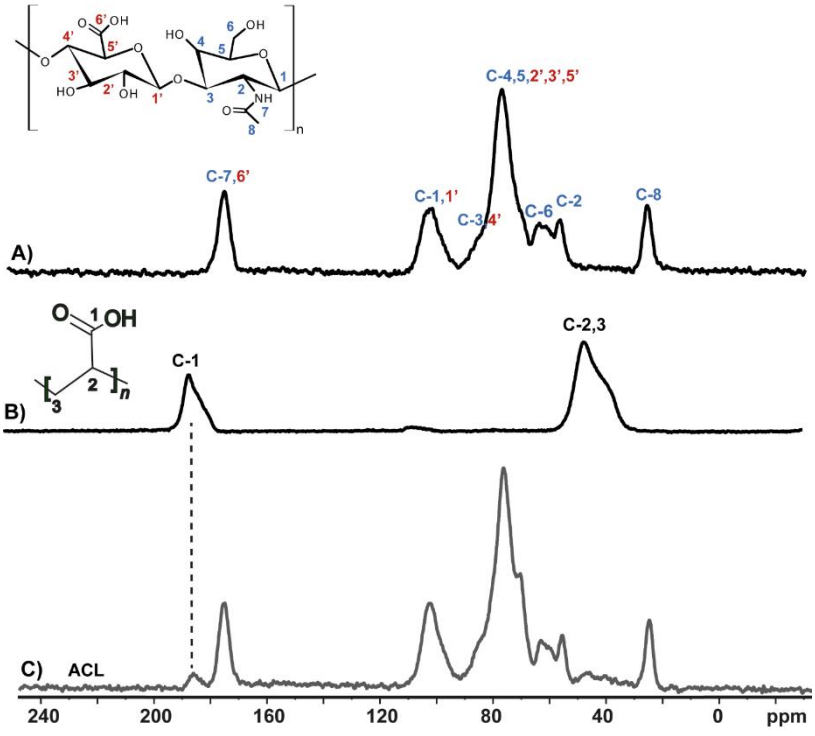

Fig. 3. ^{13}C CP-MAS NMR spectra of A) hyaluronic acid, B) carbomer and C) ACL.

Furthermore, in Fig. 4 the characteristic peaks of ACL and both ESM-SAL could be clearly observed in the single-drug (ACL-E05, ACL-S05) and dual-drugs (ACL-ES05) formulations. A comparison of ACL and ESM spectra with those of the ACL-E05 and ACL-ES05 formulations (Fig. 4 panel A) shows no changes in the chemical shifts and patterns of HA/agarose lines, whereas all peaks of ESM are broadened and the carbonyls C-5, C-4 show chemical shift changes. A chemical shift variation of 3 ppm is also observed for the carboxyl C-1 of carbomer in the ACL-E05 formulation. Similar considerations can be made by comparing the spectra of pristine SAL, ACL with those of ACL-S05 and ACL-ES05 (Fig. 4 panel B). Small variations in chemical shift are observed for C-1, C-2, C-6 of SAL and again a variation of about 3 ppm for the carboxyl C-1 of carbomer in the ACL-S05 formulation. Similar results are obtained for the ACH formulation (see Figs. SI2 and SI3). This change can be ascribed to drug-polymer interactions that occur when a singled drug is loaded. Interestingly, in ACL-S05 spectrum signal 3 of SAL is a broad singlet due to the intramolecular hydrogen bond between OH and carboxylate group, which provides a single conformation of the OH group. Conversely, in the dual drug formulation (ACL-ES05) signal 3 is a doublet arising from two different orientations of the OH-phenyl in the polymer matrix, reasonably due to the competition between the intramolecular hydrogen bond and the intermolecular SAL-ESM ones. Despite these findings, probing the intermolecular drug-drug interactions remain rather difficult due to broad lines in the ^{13}C CP-MAS spectra. Hence, more detailed information can be obtained from ^{1}H MQ MAS data.

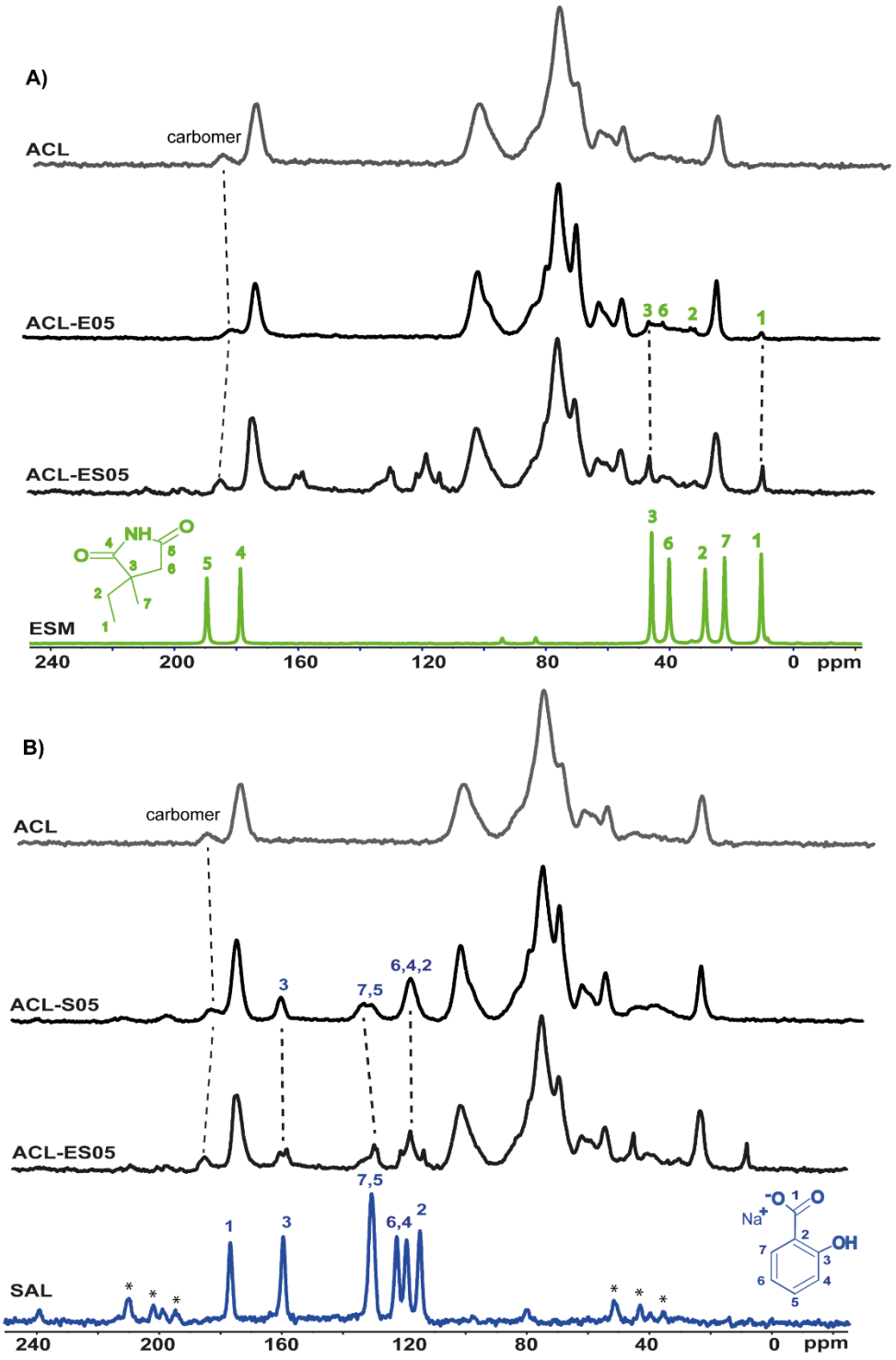

341

342 **Fig. 4.** ^{13}C CP-MAS NMR spectra of (panel A) ACL, ACL-E05, ACL-ES05, ESM; (panel B)

343 ACL, ACL-S05, ACL-ES05, SAL. Spinning sideband are marked with a *.

344

The ^{1}H single quantum (SQ) spectra for both the ACL-ES05 and ACH-ES05 samples are shown in Fig. 5A. The lineshape remains broad despite the moderately fast spinning frequency of 36 kHz, due to a combination of strong H-H interactions as well as a broad distribution of chemical shifts in the lyophilised samples. The only well resolved signal can be attributed to the weak resonance from above 12 ppm due to carboxylic protons involved in hydrogen bonds (Traer, Britten & Goward, 2007).

In an effort to further understand the proton network in this complex system we performed 2D homonuclear double-quantum measurements. Data for both samples are shown in Fig. 5B-C. For the interpretation of the 2D SQ-DQ NMR spectra, we note that while the signals in the SQ dimension appear at the usual chemical shift of the individual sites, the signals in the DQ dimension will appear at the sum of the chemical shifts between interacting species, if and only if the sites are close enough for a through-space dipolar interaction to be discernible in the timescale of the experiment. Hence, the SQ-DQ is very informative when it comes to establish proximities, determined via ^{1}H-^{1}H interactions in this case. For both samples, the aliphatic/aromatic regions are broadly similar in terms of DQ patterns. Given the size of the spin system and the fact that exact geometry and dipolar interactions between the different species are unknown, it was attempted to approximately reproduce the lineshapes via 2D Gauss-Lorentz functions. The fitted spectra, using an ensemble of 10 sites, is shown in Fig. 5D-F for both samples. Further details about the fits are provided in the ESI (Table S1 and S2). For both samples, while it is hard to over-assign peaks in these broad spectra, it is nevertheless possible to identify signal regions of interest for the purpose of the evaluation of the aliphatic-aromatic interactions. As shown in Fig. 2, ACL-E40 and ACL-S40 have only aliphatic and aromatic protons, respectively. Hence the presence of a DQ signal at the sum of the chemical shift for aliphatic and aromatic protons is a clear indication that these

368 species are very close at a molecular level. Using the peak numbering as reported in figure 5D
369 and provided in the ESI, there are well resolved signals correlating the acidic protons to their local
370 environment through hydrogen bonding (peaks near 12-14 ppm in SQ dimension, i.e, peaks 9, 10
371 of the fits). Peaks 1, 3, 4 are compatible with interactions within the aliphatic framework. More
372 interestingly, peaks 2 and 8 are compatible with a correlation between the aliphatic and aromatic
373 environments. The signal at 5 is likely an inter-aromatic signal. Moreover, peak 6 contains a
374 combination of aliphatic-acidic and aliphatic-aromatic correlations, as shown by the larger
375 confidence limits for the DQ dimension for the peak position and linewidth. Noting that we are
376 over-simplifying the peak assignment and discussion here, as the lack of resolution makes the fit
377 unstable if too many free-parameters are included in the fit, but the general trends are the presence
378 of signals compatible with an aliphatic-aromatic interaction is nevertheless rather clear. This
379 finding is in line with the selective chemical shift variation reported above for HR-MAS NMR
380 section detected on ESM protons, which have been associated to the interactions between aliphatic
381 and aromatic moieties in ESM and SAL, respectively.
382

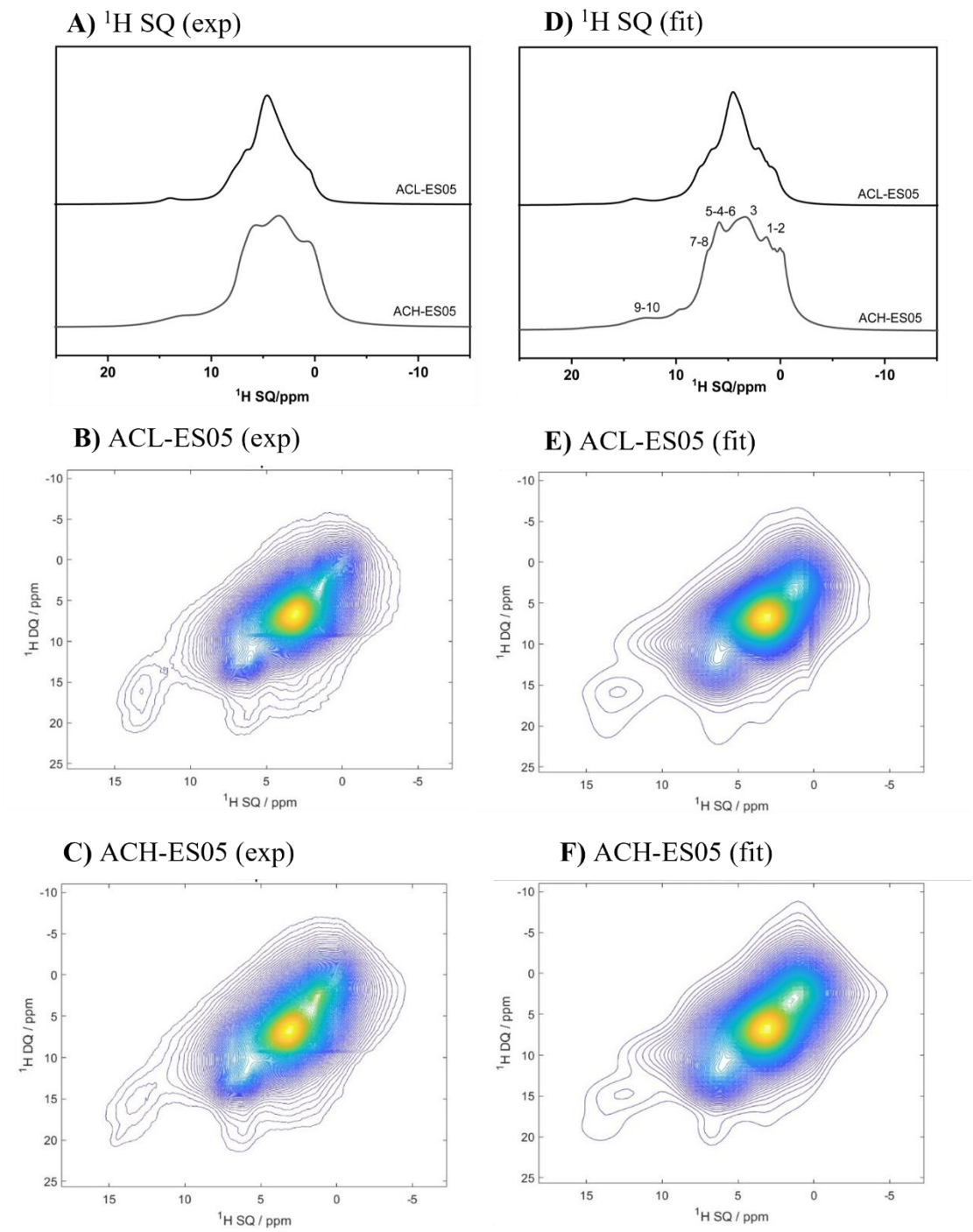

Fig. 5. ^{1}H SQ spectra of ACH-ES05 and ACL-ES05 (A). ^{1}H 2D SQ-DQ spectra of ACH-ES05 (B) and ACL ES05 (C) $\omega_r/2\pi = 36$ kHz and 8 scans. ^{1}H SQ fit for ACH-ES05 and ACL-ES05 using

10 peaks and peaks assignment (D). ^{1}H 2D SQ-DQ fit using 10 peaks for ACL-ES05 (E) and ACH-ES05 (F).

3.3 Numerical analysis of HR-MAS NMR diffusion data

In the following we shall present the analysis of our NMR diffusion data by means of the two approaches detailed in Methods section. Prior to present our results, we note that all NMR data in the present study were acquired separately for each species diffusing within the same medium. This differs from our previous approach (Vanoli et al., 2023), where both drugs were loaded individually, as stand-alone species, in water and hydrogel. The comparison with these results is of key importance to understand the effects of codelivery on drug diffusion in AC hydrogels.

3.3.1 ESM and SAL diffusion in water

To begin with, we consider the analysis of both drugs in water by means of the techniques described in the previous section, namely q-scaling and GD approaches. Table 2 collects the numerical values of the fitting parameters obtained by means of the q-scaling approach. These include the parameters α, μ, and β which are associated with the diffusion mechanism. The last three columns collect the values of the diffusion coefficients, as determined from q-scaling (K), from gaussian deconvolution (D_P), and from the standard regression approach (D_R). The value of D_P was obtained averaging over the estimates obtained at each diffusion time. Instead, D_R corresponds to the value obtained by fitting the MSD at each diffusion time, assuming Gaussian diffusion.

All the values obtained from q-scaling approach suggest both species to diffuse in water according to a Gaussian model, characterized by α close to 1 and $\mu = 2$. As previously noted, (Vanoli et al.,

2023), the values of K should not generally be compared with the diffusion coefficients obtained within Gaussian models, due to the different units. In the limit of Gaussian diffusion, K should approach that obtained with standard regression, aside from the differences related to the fitting procedure. The values of K of listed in Table 2 qualitatively resemble those of D_R within each sample. The differences are due to the functional form of Eq. (6), which makes K sensitive to the value of the other parameters.

Table 2. Numerical values of α, μ, β, and K, D_P and D_R obtained by fitting the HR-MAS NMR data of ethosuximide and salicylate in water, at 40 mg/L and 75 mg/L. D_P refers to the average diffusion coefficient, obtained averaging the estimates at each time. D_R is the Gaussian diffusion coefficient, obtained by means of standard regression.

Sample	probed drug	α	μ	β	K [m^{μ}/s^{β}]	D_P [m^2/s]	D_R [m^2/s]
WAT-ES40	ESM	1.084(26)	1.972(2)	1.069(26)	$9.74(20) \cdot 10^{-10}$	$5.72(18) \cdot 10^{-10}$	$5.906(33) \cdot 10^{-10}$
WAT-ES40	SAL	1.081(25)	2.005(8)	1.083(25)	$6.99(61) \cdot 10^{-10}$	$5.93(19) \cdot 10^{-10}$	$6.086(38) \cdot 10^{-10}$
WAT-ES75	ESM	1.093(33)	1.970(2)	1.076(33)	$8.93(19) \cdot 10^{-10}$	$4.99(19) \cdot 10^{-10}$	$5.163(54) \cdot 10^{-10}$
WAT-ES75	SAL	1.096(36)	2.002(2)	1.097(36)	$6.67(15) \cdot 10^{-10}$	$5.21(20) \cdot 10^{-10}$	$5.404(84) \cdot 10^{-10}$

The diffusion coefficients obtained by the GD approach those of standard regression. Within the GD approach, the signal intensities collected at each diffusion time are fitted independently by means of a finite set of gaussian functions with different diffusion coefficients. In principle, for an

ideal diffusive Gaussian process, the P(D) in Eq. (8) should be infinitely narrow and centred at D_P (DiSpirito et al., 2023). This outcome is not observed in practice, either due to the use of a finite number of Gaussians and intrinsic signal noise. Nonetheless, upon approaching Gaussian diffusion, we may correctly expect P(D) to be a mono-modal distribution centred at D_P. This outcome is that observed in both the samples considered, as shown in Figs. SI4 and SI5. Given the above considerations, the differences between D_P and D_R are essentially related to the fitting procedure. As we shall show below, the main strength of the GD approach is to admit the possibility of different diffusion coefficients for the same species, which is beyond the descriptive capability of standard regression techniques.

The fitting parameters listed in Table 2 for q-scaling (namely, α, μ, and β) are quite similar with those obtained for the same species in water, without codelivery (see Vanoli et al., 2023 for a comparison). A careful comparison between these data sets should account for the effects of drug concentration on the diffusion coefficients. Even so, the diffusion coefficients of co-delivered species are smaller than those previously reported. This outcome might be related with the intermolecular interactions between the two species, as evidenced by the NMR data reported in the previous section (Figs. 2 and 5).

3.3.2 ESM and SAL diffusion in hydrogels

The results obtained by fitting the PGSE NMR data with the procedure described above for ESM and SAL at 5 mg/ml loading, are reported in Table 3. Within the ACH formulation, at such low drug concentrations, both species exhibited Fickian diffusion. In ACL-loaded samples, conversely, the values of α, slightly exceeding unity, suggesting a mild superdiffusive behavior. The deconvolution of the signal intensities confirmed the above analysis. The PDFs of the two species

in ACH and ACL are reported in Figs. SI6 and SI7. For each species, at all diffusion times, we found single-peaked PDFs, with few exceptions for SAL. The PDFs associated with SAL were generally broader than those for ESM. At present, no simple interpretation justifies this outcome. The lack of systematic trends suggests these anomalies to be related to the increase of data noise on going from water to hydrogel, as reported elsewhere (Vanoli et al., 2023).

Table 3. Numerical values of α, μ, β, and K obtained by fitting the HR-MAS NMR data of ethosuximide (ESM) and salicylate (SAL) corresponding to a concentration of 5 mg/ml in all samples. For comparison purposes, the diffusion coefficients D_P and D_R, obtained by means of gaussian deconvolution and standard regression (α = 1 and μ = 2) are also reported.

Sample	probed drug	α	μ	β	K [m^{μ}/s^{β}]	D_P [m^2/s]	D_R [m^2/s]
ACH-ES05	ESM	1.047(9)	1.985(13)	1.040 (11)	$1.43(19) \cdot 10^{-9}$	$1.17(5) \cdot 10^{-9}$	$1.11(2) \cdot 10^{-9}$
	SAL	1.050(8)	1.772(15)	0.931(11)	$1.27(21) \cdot 10^{-8}$	$1.28(12) \cdot 10^{-9}$	$1.08(2) \cdot 10^{-9}$
ACL-ES05	ESM	1.181(11)	1.840(7)	1.086(11)	$1.13(8) \cdot 10^{-8}$	$1.73(18) \cdot 10^{-9}$	$1.64(5) \cdot 10^{-9}$
	SAL	1.192(6)	1.681(7)	1.002(7)	$5.27(36) \cdot 10^{-8}$	$1.55(13) \cdot 10^{-9}$	$1.49(4) \cdot 10^{-9}$

As shown in Table 4, increasing drugs concentration to 40 mg/ml had different effects on drug diffusion, depending on the hydrogel formulation. In ACH, the hydrogel with the largest mesh size, the diffusion of both species showed moderate deviations from ordinary diffusion (i.e., α = 1 and μ = 2). In ACL, such deviations were markedly larger, suggesting a superdiffusive behaviour for both drugs, characterized by α > 1 and μ < 2.

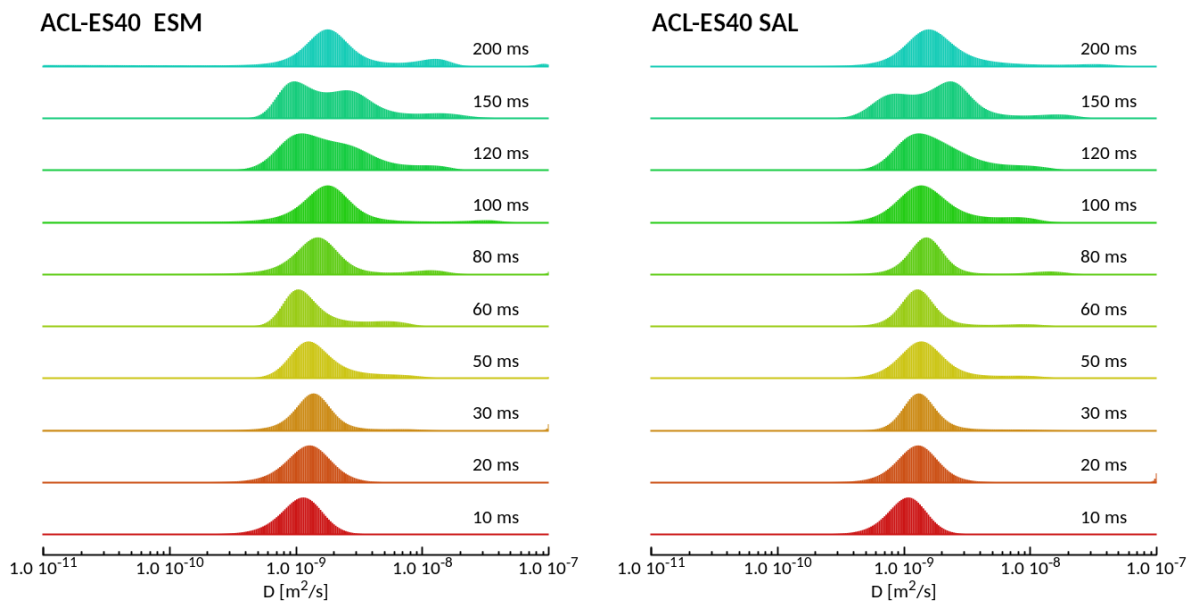

464 **Fig. 6.** Probability distribution functions obtained for ESM (left) and SAL (right) in ACL-ES40.

465

466 Consistent with the above findings, Gaussian deconvolution led to similar PDFs for the two drugs
467 in both hydrogels. This is depicted in Fig. 6 for ACL-ES40 and in Fig. SI8 for ACH-ES40. These
468 profiles are broader than those reported at 5 mg/mL (see Figs. SI6 and SI7). This effect was not
469 related to co-loading two drugs, but rather to the increase in drug concentration, as evidenced by
470 a parallel analysis carried out on the data published in our previous study (Vanoli et al., 2023).
471 In contrast to ACH-ES40 (see Fig. SI8), where all PDFs were monomodal, those of ACL-ES40
472 exhibited groups of diffusion coefficients associated with different peaks above 50 ms. The
473 inspection of the PDF profiles for other samples revealed that such features were generally absent
474 in all cases for α slightly exceeding unity (e.g. $\alpha \approx 1.1$), yet increasingly present for $\alpha > 1.2$. This
475 outcome suggests a potential connection between PDF shape and superdiffusion. However, at
476 present, it is difficult to establish a quantitative relationship, mainly due to the effect of hydrogel
477 heterogeneity on the intensity of the NMR signal.

Despite the results obtained for ACL-ES40, the diffusion coefficients obtained from standard regression, D_R, turned out to approach D_P estimates quite closely. As shown below this outcome should be considered purely incidental, since linear regression failed accurately fitting the MSD distribution.

According to the results presented so far, one visible effect of co-loading two drugs was to "equalize" the diffusive behaviour of the two species. This contrasts with the results we obtained on single-drug formulations (Vanoli et al., 2023), where the deviations of α from unity were moderate for ESM, but significant for SAL, regardless of formulation and drug concentration. The intermolecular interactions between ESM and SAL identified by NMR may be responsible for this outcome. These include aliphatic-aromatic interactions (see Figs. 2 and 5 above) and hydrogen bonding between the two species. We note that the latter is possibly hidden by the signals associated with hydrogel's acidic moieties. Nonetheless, it looks reasonable based on the chemical structures of the two drugs.

Table 4. Numerical values of α, μ, β, and K obtained by fitting the HR-MAS NMR data of ethosuximide (ESM) and salicylate (SAL) loaded with a concentration of 40 mg/ml in all samples. For comparison purposes, the diffusion coefficients D_P and D_R, obtained by means of gaussian deconvolution and standard regression (α = 1 and μ = 2) are also reported.

Sample	probed drug	α	μ	β	K [m^{μ}/s^{β}]	D_P [m^2/s]	D_R [m^2/s]
ACH-ES40	ESM	1.132(20)	1.819(3)	1.030(18)	$1.00(35) \cdot 10^{-8}$	$1.23(9) \cdot 10^{-9}$	$1.27(4) \cdot 10^{-9}$
	SAL	1.152(23)	1.819(9)	1.048(21)	$1.09(9) \cdot 10^{-8}$	$1.31(10) \cdot 10^{-9}$	$1.30(3) \cdot 10^{-9}$
ACL-ES40	ESM	1.328(23)	1.547(6)	1.027(18)	$3.79(22) \cdot 10^{-7}$	$2.53(27) \cdot 10^{-9}$	$2.65(13) \cdot 10^{-9}$

	SAL	1.256(23)	1.557(3)	0.978(18)	$2.83(9) \cdot 10^{-7}$	$2.36(19) \cdot 10^{-9}$	$2.41(11) \cdot 10^{-9}$

Table 5 summarizes our results for the samples with 75 mg/ml drug loading. The two drugs shared closely similar diffusion parameters within the same hydrogel. In both hydrogels both drugs exhibited superdiffusive dynamics. Nonetheless, similar estimates were obtained for D_P and D_R. The inspection of MSD values reported in Fig.SI10 for both drugs demonstrates that linear regression failed to capture the nonlinear relationship between MSD and time.

The PDFs for ACH-ES75 are reported in Fig. 7. Upon increasing the diffusion time, a small envelope of diffusion coefficients gradually departed from the starting one, moving toward higher values. Such PDF "splitting", already recognized in some of the previous samples, was here more regular. The position of the secondary group of coefficients changed over time, thus making D_P no longer constant. An entirely similar result was observed for ACL-ES75 (see Fig. SI9).

The diffusion parameters obtained for ACH-ES75 (see Table 5) deserve a final comment. In all other samples we found $\alpha > 1$, $\mu < 2$, and $\beta = 1$, corresponding to commonly observed superdiffusion (Yang, Reutens, & Vegh, 2022). Conversely, in the case of ACH-ES75 we found $\beta > 1$ for both drugs. This suggests that the transport dynamics may involve trapping-release events, at least for the fraction molecules for which time-varying diffusion coefficients were observed. Below, we provide a possible interpretation for this phenomenon.

Table 5. Numerical values of α, μ, β, and K obtained by fitting the HR-MAS NMR data of ethosuximide (ESM) and salicylate (SAL) loaded with a concentration of 75 mg/ml in all samples.

For comparison purposes, the diffusion coefficients D_P and D_R, obtained by means of gaussian deconvolution and standard regression ($\alpha = 1$ and $\mu = 2$) are also reported.

Sample	probed drug	α	μ	β	K [m^{μ}/s^{β}]	D_P [m^2/s]	D_R [m^2/s]
ACH-ES75	ESM	1.362(17)	1.773(8)	1.207(16)	$3.25(25) \cdot 10^{-8}$	$1.41(13) \cdot 10^{-9}$	$1.62(6) \cdot 10^{-9}$
	SAL	1.383(20)	1.763(7)	1.219(19)	$3.88(27) \cdot 10^{-8}$	$1.45(15) \cdot 10^{-9}$	$1.78(10) \cdot 10^{-9}$
ACL-ES75	ESM	1.328(27)	1.505(3)	0.999(20)	$4.53(15) \cdot 10^{-7}$	$1.87(17) \cdot 10^{-9}$	$1.78(6) \cdot 10^{-9}$
	SAL	1.342(22)	1.601(7)	1.074(18)	$1.82(13) \cdot 10^{-7}$	$1.71(16) \cdot 10^{-9}$	$1.83(7) \cdot 10^{-9}$

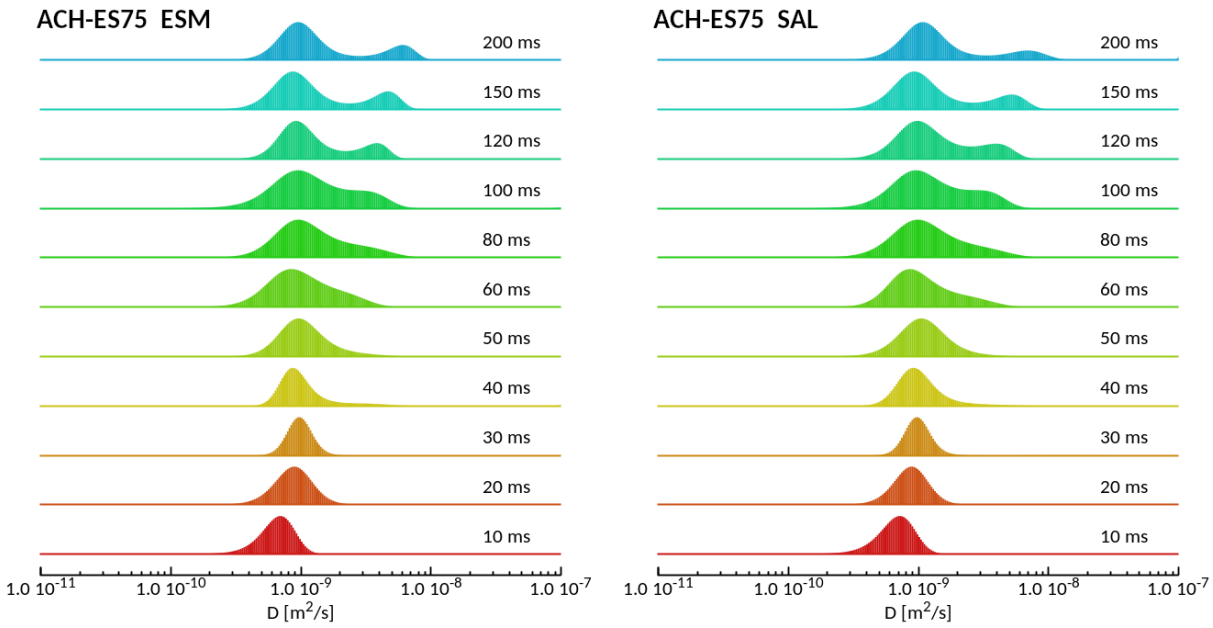

Fig.7. Probability distribution functions obtained for ESM (left) and SAL (right) in ACH-ES75.

3.4 Drug release kinetics

To investigate the effect of intermolecular drug-drug interactions on the release kinetics in dual therapeutic loads, samples of ACL-ES05 and ACH-ES05 were analysed. The cumulative release profiles of both drugs are displayed in Fig. 8.

A significant amount of both drugs was released from ACL (~34% for ESM and ~53% for SAL) and ACH (~51% for ESM and ~54% for SAL) already after 30 minutes. Within 5 hours, the amount of drugs released reached 63% for ESM and 96% for SAL in ACL hydrogels. Similar percentages were observed in ACH gels: 67% for ESM and 96% for SAL, respectively.

These release profiles were comparable to those obtained for the single-drug formulations in our previous work (Vanoli et al., 2023), except for ESM, showing asymptotically a partial rather than a complete release. This result indicates that a significant fraction of the drug (more than 30%) remains inside the hydrogel network. This outcome has also been observed in other systems [Hu et al., 2020; Han et al., 2010; Pan et al., 2016]. At present, it has no simple explanation and will be the subject of future works.

To identify potential analogies between the release kinetics and the diffusion mechanisms outline above, we attempted at fitting our release data considering the cylindrical shape of the samples and assuming both drugs homogeneously distributed within the hydrogel. A former attempt, made with a model adopted in our previous work (Castiglione et al., 2019) failed due to the fast release kinetics of both drugs. A second attempt was then carried out using a mono-dimensional model based on Fick's laws (Rossi et al., 2015). The results, reported in Fig. SI11, were satisfactory for both drugs, although the model was not able to fully capture ESM release profile. The diffusion coefficients obtained from the fitting were $3.45 \cdot 10^{-9}$ m^2/s and $4.03 \cdot 10^{-9}$ m^2/s for ESM in ACL and ACH, respectively, whereas $1.22 \cdot 10^{-8}$ m^2/s and $1.01 \cdot 10^{-8}$ m^2/s for SAL. These values are higher

than those obtained from fitting NMR data, possibly suggesting different mechanisms for diffusion and release.

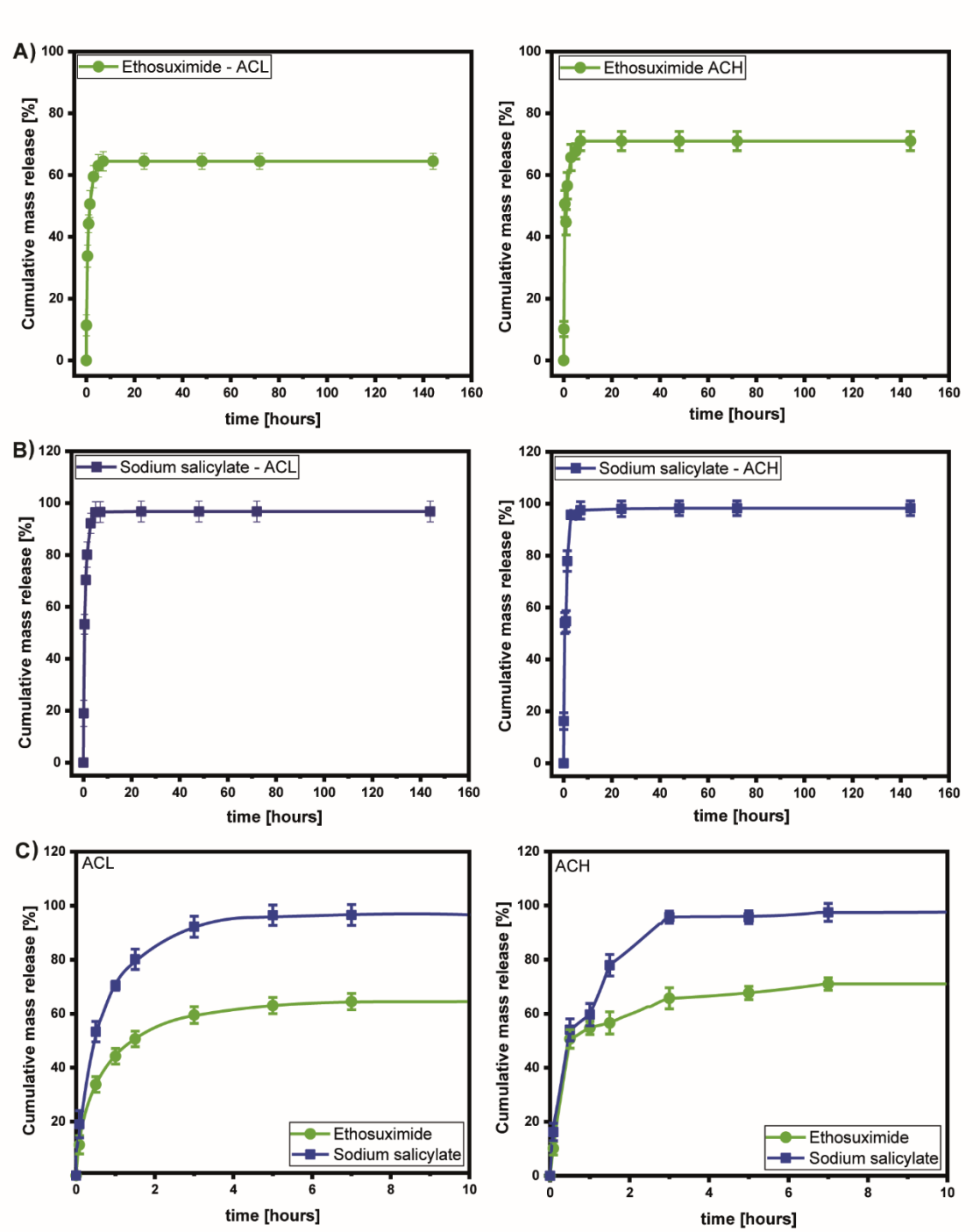

Fig. 8. Cumulative mass release for the codelivery of ESM (A) and SAL (B) from hydrogels ACL (*left*) and ACH (*right*) at 37° C. Close comparison of release profiles from ACL *(left)* and ACH *(right)* for both drugs (C).

3. Conclusions

In this study, we investigated the effects of co-loading two drugs, ethosuximide and salicylic acid on their diffusion motion and release from hyaluronic acid-based hydrogels. The two drugs considered are "orthogonal" in terms of pharmacological use and chemical structure. Ethosuximide is an aliphatic compound used to treat epilepsy. Salicylic acid, conversely, is an aromatic compound with well-recognized anti-inflammatory capabilities. The choice of these drugs, mostly based on the availability of data collected by our group on analogous single-drug formulations (Vanoli et al., 2023), aimed at proposing a simultaneous therapy for different diseases. At variance with our previous results on single-drug formulations, we found for both drugs similar diffusion dynamics within the hydrogel network, at all drug loadings. Our NMR data suggest this outcome to be associated with the intermolecular interactions between the aliphatic and aromatic moieties of ESM and SAL, respectively. Although, at present, we cannot provide further evidence in support of this conclusion, we note that such "CH-π" interactions may eventually be stronger than aromatic-aromatic ones (Kim, Karthikeyan, & Singh, 2011), and their impact on drug diffusion should not be overlooked. Based on the chemical structures of the two compounds, hydrogen bonding between the two species is not unlikely, although difficult to assess experimentally due to the signals associated with hydrogel's acidic moieties.

Equally interesting is the splitting of the diffusion coefficient distributions clearly observed in the samples with highest drug loading (75 mg/mL). This outcome may be related to the existence of two main groups of molecules diffusing differently, owing to different local environments. A

tentative interpretation is as follows. At low drug loadings, molecular diffusion is slow and essentially dominated by drug-hydrogel interactions, consistently with ^{13}C CP-MAS NMR measurements. As evidenced by ^{1}H SQ and SQ-DQ experiments, these interactions can be associated with hydrogen bonding between the drugs and the polymer.

Increasing drug loading saturates an increasingly larger fraction of hydrogel interaction sites. The remaining fraction of molecules is free to diffuse in the water phase. Due to dilution, the diffusion coefficient of such molecules is higher than that of their "bound" analogues. The shift of these diffusion coefficients over time implies a time-dependent diffusion mechanism, which may be related to the interactions mentioned above, but was never observed before and remains to be clarified. Further efforts will also be dedicated to better understand the connection between diffusion and release mechanisms. These might be different, as indicated by release data fitting. We believe that further developments of existing release models will be necessary to test this hypothesis.

Compared to single drug formulations, codelivery profiles show a decrease of the maximum amount of ethosuximide released from the hydrogel. Once explained, this outcome will possibly improve our current understanding, adding more options to the development of dual-drug delivery systems.

Appendix A. Supplementary data

Supplementary data to this article can be found online.

Acknowledgments

We acknowledge the support from the International Exchange program of the Royal Society of Chemistry, grant number IES\R1\211163.

References

Adepu, S. and Ramakrishna, S. (2021). Controlled drug delivery systems: current status and future directions. *Molecules, 26*, 5905.

Amann, R., Peskar, B. A. (2002). Anti-inflammatory effects of aspirin and sodium salicylate. *European Journal of Pharmacology, 447,* 1-9,

Axpe, E., Chan, D., Offeddu, G. S., Chang, Y., Merida, D., Lopez Hernandez, H. and Appel, E. A. (2019). A Multiscale Model for Solute Diffusion in Hydrogels. Macromolecules, 52, 6889-6897.

Bachmann, K. A., Jauregui, L. (1993). Use of single sample clearance estimates of cytochrome P450 substrates to characterize human hepatic CYP status in vivo. *Xenobiotica, 23(3),* 307-315

Bajpai, A. K., Shukla, S. K., Bhanu, S., Kankane, S. (2008). Responsive polymers in controlled drug delivery. *Progress in Polymer Science, 33*, 1088-1118.

Burmester, G. R., Pope, J. E. (2017). Novel treatment strategies in rheumatoid arthritis. *Lancet, 389*, 2338-2348.

Casalegno, M., Raos, G., Appetecchi, G.B., Passerini, S., Castiglione, F., Mele, A. (2017). From nanoscale to microscale: crossover in the diffusion dynamics within two pyrrolidinium-based ionic liquids. *Journal of Phys. Chem. Lett., 8*, 5196-5202.

Castiglione, F., Casalegno, M., Ferro, M., Rossi, F., Raos, G. and Mele A. (2019). Evidence of superdiffusive nanoscale motion in anionic polymeric hydrogels: Analysis of PGSE- NMR data and comparison with drug release properties. *J. Controlled Release, 305*, 110-119.

Chen, B., Miller, R. J., Dhal, P. K. (2014). Hyaluronic acid-based drug conjugates: state-of-the-art and perspectives. *J Biomed Nanotechnol., 10*, 4-16.

Choi, K., Myoung, S., Seo, Y. and Ahn, S. (2021). Quantitative NMR as a versatile tool for the reference material preparation. *Magnetochemistry, 7*, 15.

Di Spirito, N. A.; Grizzuti, N.; Casalegno, M.; Castiglione, F.; Pasquino, R. (2023). Phase transitions of aqueous solutions of Pluronic F68 in the presence of Diclofenac Sodium. *International Journal of Pharmaceutics, 644*, 123353.

Fick, A. (1855). Ueber Diffusion. *Ann. Phys*., *170*, 59-86.

Fraser, J. R. E., Laurent, T. C., & Laurent, U. B. G. (1997). Hyaluronan: Its nature, distribution, functions and turnover. *Journal of Internal Medicine, 242(1)*, 27–33.

Gadde, S. (2015). Multi-drug delivery nanocarriers for combination therapy. *Med. Chem. Comm. 6*, 1916-1929.

Giaccone, M., Bartoli, A., Gatti, G., Marchiselli, R., Pisani, F., Latella, M. A., Perucca, E. (1996). Effect of enzyme inducing anticonvulsants on ethosuximide pharmacokinetics in epileptic patients. *Br. J. Clin. Pharmacol. 41(6)*, 575-579.

Hamedi, H., Moradi, S., Hudson, S. M., Tonelli, A. E. (2018). Chitosan based hydrogels and their applications for drug delivery in wound dressings: A review. *Carbohydrate Polymers, 199*, 445–460.

Han, Y.; Shchukin, D.; Fernandes, P.; Mutihac, R.-C.; Möhwald, H. Mechanism and kinetics of controlled drug release by temperature stimuli responsive protein nanocontainers. (2010). *Soft Matter, 6*, 4942–4947.

Hassan, W., Dong, Y., Wang, W. (2013). Encapsulation and 3D culture of human adipose-derived stem cells in an in-situ crosslinked hybrid hydrogel composed of PEG-based hyperbranched copolymer and hyaluronic acid. *Stem Cell Research & Therapy, 4*, 32.

Hoffman, A. S. (2008). The origins and evolution of "controlled" drug delivery systems. *Journal of Controlled Release, 132*, 153-163.

Hu, Q., Sun, W., Wang, C., Gu, Z. (2016). Recent advances of cocktail chemotherapy by combination drug delivery systems. *Advanced Drug Delivery Reviews, 98*, 19-34.

Huang, G., Huang, H. (2018). Application of hyaluronic acid as carriers in drug delivery. *Drug Delivery, 25*, 766-772.

Hu, X.; Wang, Y.; Zhang, L.; Xu, M. (2020). Formation of self-assembled polyelectrolyte complex hydrogel derived from salecan and chitosan for sustained release of Vitamin C. *Carbohydr. Polym. 234*, 115920.

Khunmanee, S., Jeong, Y. and Park, H. (2017). Crosslinking method of hyaluronic-based hydrogel for biomedical applications. *Journal of Tissue Engineering, 8*, 1-16.

Ji, L., Zhang, F., Zhu, L., Jiang, J. (2021). An in-situ fabrication of bamboo bacterial cellulose/sodium alginate nanocomposite hydrogels as carrier materials for controlled protein drug delivery. *International Journal of Biological Macromolecules, 170*, 459–468.

Kim, K. S., Karthikeyan, S. and Singh, N. J. (2011). How Different Are AromaticπInteractions from AliphaticπInteractions and Non-πStacking Interactions? *J.Chem.Theory Comput., 7*, 3471-3477.

Jia, J., Zhu, F., Ma, X., Cao, Z. W., Li, Y. X., Chen, Y. Z. (2009). Mechanisms of drug combinations: interaction and network perspectives. *Nat. Rev. Drug Discov., 8*, 111-128.

Jiang, D., Liang, J., Noble, P. W. (2011). Hyaluronan as an Immune Regulator in Human Diseases. *Physiol. Rev., 91*, 221–264.

Lapčík, L., Lapčík, L., De Smedt, S., Demeester, J., Chabreček, P. (1998). Hyaluronan: preparation, structure, properties, and applications. *Chem. Rev., 98*, 2663-2684.

Levitt, M. H. (2002). Symmetry-Based Pulse Sequences in Magic-Angle Spinning Solid-State NMR. *Encyclopedia of Nuclear Magnetic Resonance: Advances in NMR, 9*, 165-196.

Lucy, L. B. (1974). An iterative technique for the rectification of observed distributions. *Astronomical Journal, 79*, 745.

Lv, Z., Chang, L., Long, X., Liu, J., Xiang, Y., Liu, J., Liu, J., Deng, H., Deng, L., Dong, A. (2014). Thermosensitive in situ hydrogel based on the hybrid of hyaluronic acid and modified PCL/PEG triblock copolymer. *Carbohydrate Polymers, 108*, 26-33.

Madau, M., Morandi, G., Lapinte, V., Le Cerf, D., Dulog, V., Picton, L. (2022). Thermo-responsive hydrogels from hyaluronic acid functionalized with poly(2-alkyl-2-oxazoline) copolymers with tuneable transition temperature. *Polymer, 244*, 124643.

Meng, Q. Y., Cong, H. L., Hu, H., Xu, F. J. (2020). Rational design and latest advances of codelivery systems for cancer therapy. *Materials Today Bio, 7*, 100056.

Metzler, R., Klafter, J. (2000). The random walk's guide to anomalous diffusion: a fractional dynamics approach. *Phys. Rep., 339* (1), 1-77.

Noreen, S., Pervaiz, F., Ijaz M. & Shoukat, H. (2022) Synthesis and characterization of pH-sensitive chemically crosslinked block copolymer [Hyaluronic acid/Poloxamer 407-co-poly (Methacrylic acid)] hydrogels for colon targeting. *Polymer-Plastics Technology and Materials, 61*, 1071–1087.

Pan, G.; Bao, Y.-J.; Xu, J.; Liu, T.; Qiu, Y.-Y.; Shi, X.-J.; Yu, H.; Jia, T.-T.; Yuan, X.; Yin, P.-H.; and Cao, Y. J. (2016). Esterase-responsive polymeric prodrug-based tumor targeting nanoparticles for improved anti-tumor performance against colon cancer. *RSC Adv., 6*, 42109-42119.

Patt, S. L. (1982). Pulse strategies for the suppression of acoustic ringing, *J. Magn. Reson., 49*, 161-163.

Perale, G., Rossi, F., Santoro, M., Marchetti, P., Mele, A., Castiglione, F., Raffa, E., Masi, M. (2011). Drug release from hydrogel: a new understanding of transport phenomena, *J. Biomed. Nanotechnol., 7*, 476-481.

Perez, L. A., Hernandez, R., Alonso, J. M., Perez-Gonzalez, R., & Saez-Martínez, V. (2021). Hyaluronic acid hydrogels crosslinked in physiological conditions: Synthesis and biomedical applications. *Biomedicines, 9*, 1113.

Pizzetti, F., Maspes, A., Rossetti, A., Rossi, F. (2021). The addition of hyaluronic acid in chemical hydrogels can tune the physical properties and degradability. *European Polymer Journal, 161*, 110843.

Patsalos, P. N., Berry, D. J., Bourgeois, B. F., Cloyd, J. C, Glauser, T. A., Johannessen, S. I., Leppik, I. E., Tomson, T., Perucca, E. (2008). Antiepileptic drugs--best practice guidelines for therapeutic drug monitoring: a position paper by the subcommission on therapeutic drug monitoring, ILAE Commission on Therapeutic Strategies. *Epilepsia, 49(7),* 1239-1276.

Rampratap, P., Lasorsa, A., Perrone, B., van der Wel, P. C. A., Walvoort, M. T. C. (2023). Production of isotopically enriched high molecular weight hyaluronic acid and characterization by solid-state NMR. *Carbohydrate Polymers 316*, 121063

Rial-Hermida, M. I., Rey-Rico, A., Blanco-Fernandez, B., Carballo-Pedrares, N., Byrne, E. M., and Mano, J. F. (2021). Recent progress on polysaccharide-based hydrogels for controlled delivery of therapeutic biomolecules. *ACS Biomater. Sci. Eng.*, *7*, 4102-4127.

Richardson, W. H. (1972). Bayesian-Based Iterative Method of Image Restoration. *Journal of the Optical Society of America*. *62*, 55-59.

Rossi, F., Castiglione, F., Ferro, M., Marchini, P., Mauri, E., Moioli, M., Mele, A., Masi, M. (2015). Drug–polymer interactions in hydrogel-based drug-delivery systems: an experimental and theoretical study. Chem. Phys. Chem. *16*, 2818-2825.

Sahranavard, M., Zamanian, A., Ghorbani, F., Shahrezaee, M. H. (2020). A critical review on three dimensional-printed chitosan hydrogels for development of tissue engineering. *Bioprinting*, *17*, e00063.

Scott, J.E., Cummings, C., Brass, A., Chen, Y. (1991). Secondary and tertiary structures of hyaluronan in aqueous solution, investigated by rotary shadowing-electron microscopy and computer simulation. Hyaluronan is a very efficient network-forming polymer. Biochem. J., 274, 699-705.

Scott, J.E., Heatley, F. (1999). Hyaluronan forms specific stable tertiary structures in aqueous solution: A ^{13}C NMR study. *Proc. Natl. Acad. Sci. USA*, *96*, 4850-4855.

Sethi, S., Saruchi, Kaith, B.S., Kaur, M., Sharma, N. & Kumar, V. (2020). Cross-linked xanthan gum–starch hydrogels as promising materials for controlled drug delivery. *Cellulose, 27*, 4565-4589.

729 Stejskal, E.O. and Tanner, J.E. (1965) Spin Diffusion Measurements: Spin Echoes in the Presence
730 of a Time Dependent Field Gradient. *The Journal of Chemical Physics, 42*, 288-292.
731 Traer, J. W., Britten, J. F., Goward G. R. (2007) A Solid-State NMR Study of Hydrogen-Bonding
732 Networks and Ion Dynamics in Benzimidazole Salts. *J. Phys. Chem.*, *111*, 5602-5609
733 Vachon, M. G., Nairn, J. G. (1998). The use of ^{13}C solid state NMR to elucidate physico–chemical
734 association in Eudragit RS100 microencapsulated acyl esters of salicylic acid. *European Journal*
735 *of Pharmaceutics and Biopharmaceutics, 45*, 9-21.
736 Vanoli, V., Delleani, S., Casalegno, M., Pizzetti, F., Makvandi, P., Haugen, H., Mele, A., Rossi,
737 F., Castiglione, F. (2023). Hyaluronic acid-based hydrogels: drug diffusion investigated by HR-
738 MAS NMR and release kinetics. *Carbohydrate Polymers, 301*, 120309.
739 van Wieringen, A., Vrijlandt, C. M. (1983). Ethosuximide intoxication caused by interaction with
740 isoniazid. *Neurology, 33(9)*, 1227-1228.
741 Vargason, A. M., Anselmo, A. C. and Mitragotri, S. (2021). The evolution of commercial drug
742 delivery technologies. *Nature Biomedical Engineering, 5*, 951-967.
743 Venoruso, V., Petillo, E., Pizzetti, F., Orro, A., Comolli, D., De Paola, M. Verrillo A., Baggiolini,
744 A., Botaro, S., Castiglione, F., Sponchioni, M., Forloni, G., Rossi, F., Veglianese, P. (2024).
745 Synergistic Pharmacological Therapy to Modulate Glial Cells in Spinal Cord Injury. *Advanced*
746 *Materials, 36*, 2307747.
747 Wu, D., Chen, A., and Johnson, C. (1995). An Improved Diffusion-Ordered Spectroscopy
748 Experiment Incorporating Bipolar-Gradient Pulses. *Journal of Magnetic Resonance Series A, 115*,
749 260-264.
750 Zhang, N., Xue, L., Yunas, A., Liu, F., Sun, J., Dong, Z., Zhao, Y. (2023). Co-delivery of
751 triamcinolone acetonide and verapamil for synergistic treatment of hypertrophic scars via

carboxymethyl chitosan and Bletilla striata polysaccharide-based microneedles. *Carbohydrate Polymers, 278*, 118943.

Zong, S., Wen, H., Lv, H., Li, T., Tang, R., Liu, L., Jiang, J., Wang, S., Duan, J. (2022). Intelligent hydrogel with both redox and thermo-response based on cellulose nanofiber for controlled drug delivery. *Carbohydrate Polymers, 284*, 119219.